Author's Accepted Manuscript

Green synthesis of silver nanoparticles aimed at improving theranostics

José Vedelago, Cesar G. Gomez, Mauro Valente, Facundo Mattea

Cite this article as: José Vedelago, Cesar G. Gomez, Mauro Valente and Facundo Mattea, Green synthesis of silver nanoparticles aimed at improving theranostics, *Radiation Physics and Chemistry*, https://doi.org/10.1016/j.radphyschem.2018.01.001

Green synthesis of silver nanoparticles aimed at improving theranostics

José Vedelago[a,b,*], Cesar G. Gomez[c,d], Mauro Valente[a,b,e], Facundo Mattea[b,c,d]

[a]Instituto de Física Enrique Gaviola (IFEG), CONICET, Córdoba, Argentina.
[b]Laboratorio de Investigación e Instrumentación en Física Aplicada a la Medicina e Imágenes por Rayos X, FaMAF-UNC, Córdoba, Argentina.
[c]Dpto. de Química Orgánica, FCQ-UNC, Córdoba, Argentina.
[d]Instituto de Investigación y Desarrollo en Ingeniería de Procesos y Química Aplicada (IPQA), CONICET, Córdoba, Argentina.
[e]Centro de Física e Ingeniería en Medicina - CFIM & Departamento de Ciencias Físicas, Universidad de La Frontera, Temuco, Chile.

Abstract

Nowadays, the combination of diagnosis and therapy, known as theranostics, is one of the keys for an optimal treatment for cancer diseases. Theranostics can be significantly improved by incorporating metallic nanoparticles that are specifically delivered and accumulated in cancerous tissue. In this context, precise knowledge about dosimetric effects in nanoparticle-infused tissues as well as the detection and processing of emerging radiation are extremely important issues. In the last years the first studies on theranostic nanomaterials in gel dosimetry have been presented but there is still a broad field of study to explore. Most of gel dosimetric materials are extremely sensible to modifications in their composition, the addition of enhancers, metallic or inorganic charges can alter their stability and dosimetric properties; therefore, thorough studies must be made before the incorporation of any type of modifier. In this work, the synthesis of metallic nanoparticles suitable for gel dosimetry for x-ray applications is presented. A green synthesis process of silver nanoparticles coated with porcine skin gelatin by thermal reduction of silver nitrate is presented.

*Corresponding author
  Email address: jvedelago@famaf.unc.edu.ar (José Vedelago)
  URL: www.liifamirx.famaf.unc.edu.ar/members/vedelago/ (José Vedelago)

Nanoparticles were obtained and purified for their application in gel dosimetry. Also, nanoparticles size distribution, reaction yield and the preliminar application as theranostic agents were tested in Fricke gel dosimetry in the keV range. The obtained nanoparticles were successfully used in theranostic applications acting as fluorescent agents and dose enhancers in X-ray beam irradiation simultaneously.

1. Introduction

Relevance of nanomaterials has exponentially grown in the last twenty years in almost all health, industrial, food industry and other applications [1, 2, 3, 4]. In particular, the inclusion of nanotechnology in medicine has been an area

5 with great impact and interest in the past years [5, 6]. Nanoparticles technology has been proposed and used in medical applications such as drug delivery, antimicrobial agents, tissue engineering and theranostics [7, 8, 9]. Noble metals nanoparticles have particular interest in biomedicine due to its high atomic number, compared to soft tissue, allowing characteristic X-rays to be detected

10 outside the body [10]. Due to fluorescent emission excited in metallic nanoparticles by incident X-rays, it is possible to determine nanoparticle location and spatial distribution within an irradiated volume [11], thus improving medical practices by increasing image contrast [12] and producing local dose enhancement [13, 14].

15 Precise knowledge of the dosimetric effects due to the presence of nanoparticles becomes mandatory before considering their implementation in radiology applications. For that purpose, gel dosimetry represents a promising tool due to its three-dimensional capability and tissue equivalence [15]. Furthermore, the addition of inorganic salts and particles could turn gel dosimeters unstable

20 [16] and the compatibilization of the nanoparticles with the dosimetric material must be considered in the material design. There are many methods for the production and desing of nanoparticles, most of them are generally costly, energy

2

intensive or harmful to human and environment. Therefore, environmentally friendly procedures should be developed [17]. For example, the use of stabiliz-

₂₅ ers plays an important role in the control of metallic nanoparticles formation during the synthesis process [18], which also provides some degree of compatibility with typical dosimetry materials. Other authors use different materials for the synthesis and for the stabilization of the final products, like sodium borohydride and chitosan respectively [19], that could be not entirely environmentally

₃₀ friendly. In this work, a green method in which porcine skin collagen is used as reducing and stabilizing agent in the silver nanoparticles (Ag NPs) synthesis. The gelatin amino groups act as nucleation centers for silver ions reduction and the structural conformation of gelatin gives stability to the colloidal system of nanoparticles. In this way, the stabilizing agent already present in the dosime-

₃₅ ter exhibits less interactions and alterations of the Fricke gel dosimeters. The most significant variables considered hereby for the nanoparticles synthesis are the reagents concentrations and the reaction time. The influence of these variables on the nanoparticles dimensions, size distribution and reaction yield was evaluated in this study.

₄₀ In summary, the main goal of this work is to synthesize Ag NPs in porcine skin gelatin for theranostics applications and to evaluate the synthesis conditions to obtain suitable nanoparticles for Fricke gel dosimetry.

2. Experimental

2.1. Nanoparticles synthesis

₄₅ For the synthesis of Ag NPs, an aqueous solution of gelatin (250 Bloom purchased from Sigma Aldrich, Saint Louis, MO, USA) and an aqueous solution of silver nitrate (99.9 % acquired from Prodesa S.C.A., Buenos Aires, Argentina) were mixed to obtain the desired final concentration. Firstly, the gelatin solution was kept at 35 ℃ during 20 minutes with continuous stirring. Then, both

₅₀ solutions were mixed and stirred for 60 minutes at room temperature without any exposition to light. Once a homogeneous solution was obtained, reactors
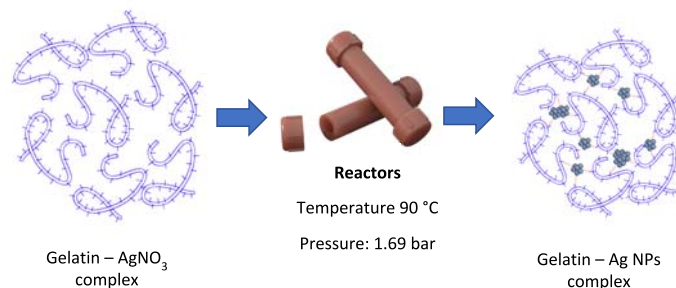
3

Figure 1: Ag NPs synthesis process.

of 25 mL volume made of polypropylene were filled with 15 mL of the reaction mixture, sealed and kept at (90 ± 1) ℃ for different reaction times in a controlled thermal bath. A graphic representation of the synthesis process is shown in

55 Figure 1. The concentrations and reaction times used in all the experimental section of this study are detailed in Table 1. The gelatin concentration effect was studied in experiments G1 to G6, the reaction time effect in experiments G1-T1 to G1-T3 and in experiments G2-T1 to G2-T3, and the silver nitrate concentration effect in experiments A1 to A3.

60 *2.2. Purification process*

A post-reaction purification process was necessary to eliminate the remaining silver ions from the products for their further use in Fricke gel dosimetry [16]. For this purpose, 5 mL of the synthesis product containing a mixture of Ag NPs, silver ions and gelatin was dialyzed during a total time of 45 hours in 500 mL.

65 Milli-Q grade water was used in the dialysis process replacing it periodically, at least four times. Benzoylated dialysis tubing with a 2000 molecular weight cutoff (MWCO) purchased from Sigma Aldrich (D7884) was used. Afterwards, a lyophilization process was carried at -48 ℃ and 0.01 mbar for 24 hours (L-T8 RIFICOR, Argentina), obtaining a dry product without altering the morphology

70 of the gelatin-silver complex material.

4

Table 1: Synthesis conditions of Ag NPs: gelatin concentration, silver nitrate concentration and reaction time.

Studied variable	Synthesis ID	AgNO$_3$ [mM]	Gelatin [mM]	Reaction time [h]
Purification	G5	150	48	15
process	G5 - dialyzed	150	48	15
	G5 - lyophilized	150	48	15
Reaction	G1 - T1	50	8	15
time	G1 - T2	50	8	24
variation	G1 - T3	50	8	48
	G2 - T1	50	16	15
	G2 - T2	50	16	24
	G2 - T3	50	16	45
AgNO$_3$	A1	25	16	15
variation	A2	50	16	15
	A3	100	16	15
Gelatin	G1	50	8	15
concentration	G2	50	16	15
variation	G3	50	24	15
	G4	150	24	15
	G5	150	48	15
	G6	150	71	15

2.3. Reaction yield estimation method

The yield of the nanoparticles synthesis was determined by a quantification consisting on obtaining the concentration of the unreacted silver ions in the final product with ascorbic acid (p.a. from Anedra, Argentina). A sample was mixed with a solution of ascorbic acid in acetic acid buffer with a pH of 4 at 25 ℃ to reduce the silver ions according to the following stoichiometry:

$$2Ag^+ + C_6H_8O_6 \rightarrow 2Ag + C_6H_6O_6 + 2H^+$$
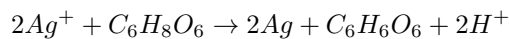
The obtained Ag NPs suspension was then centrifuged in a Rolco CM-2050 (Argentina) to separate the metallic silver from the ascorbic acid solution and the remaining ascorbic acid concentration was measured by UV-Vis spectroscopy in
₇₅ a Shimadzu UV-1800 spectrophotometer (Japan). A detailed method description was included as supplementary information in Appendix A.

2.4. TEM images analysis

Nanoparticles size distribution and morphology were characterized by transmission electron microscopy (TEM), using a JEM-JOEL 1200-EX II TEM mi-
₈₀ croscope (USA) at a 80 kV voltage, mean beam current of 58 A and vacuum of 0.3 Pa. For these analyses, synthesis reaction products were diluted in a 1:10 volumetric ratio with milli-Q water or with a 1:30 ratio for the more concentrated products (with initial 150 mM of $AgNO_3$), and placed in carbon-formvar-covered grid (Prod. No. 5624, TED PELLA INC, Sweden). The obtained TEM im-
₈₅ ages were analyzed using the procedure described elsewhere [20] using the open source software ImageJ [21]. In the present study, the diameter of a circle with equivalent area (area equivalent diameter) was used to represent the nanoparticles size distribution. At least ten different random regions of each sample grid were collected and further analyzed. A statistical analysis was performed
₉₀ with the statistical toolbox in MATLAB version 9.1.0.441655 (R2016b) 64 Bit (MathWorks Inc, Natick, MA, USA) and continuous functions were fitted to the obtained histograms. To evaluate the goodness of each fit, the Kolmogorov-Smirnov test was used [22].

2.5. UV-Vis spectroscopy

₉₅ A Shimadzu UV-1800 spectrophotometer was used to measure extinction signal of Ag NPs in an aqueous solution. Samples were placed in quartz spectroscopy cuvettes and measured from 200 to 1100 nm at room temperature. All reaction samples were diluted in milli-Q water with the same volume ratio used in the TEM analysis. The characteristic band of surface plasmon resonance was
₁₀₀ studied from the obtained spectra.

6

2.6. Dynamic light scattering

A Delsa Nano C Particle Analyzer (Beckman Coulter Inc., Brea, CA, USA), was used for the dynamic light scattering (DLS) characterization of the gelatin macromolecular structure. Measurements were made by placing the diluted ₁₀₅ samples in quartz vials at room temperature. Two hundred scans were made and averaged for each measured sample.

2.7. Fricke gel dosimetry

Fricke gel dosimeters were manufactured according to the method described elsewhere [23, 24]. Their xylenol orange concentration was set to 70 ppm to ₁₁₀ reduce any interference with the Ag NPs plasmonic signal. The lyophilized Ag NPs product was added to the dosimeters in the desired concentrations. PMMA cuvettes of $10\times10\times45$ mm^3 were used as dosimeters containers. Dose-response was characterized by means of optical methods.

2.8. X-ray irradiations

₁₁₅ Two different setups were used in this study. Firstly, the feasibility of using Ag NPs as a dopant agent for dose enhancement was studied. For that purpose, Fricke gel dosimeters containing Ag NPs were irradiated with an X-ray tube coupled to a W anode and a Kristallofex (Siemens) generator with a maximum power of 3 kW. Two different incident beams were used maintaining the ₁₂₀ dose rate at (259 ± 1) mGy/min, which was measured by calibrated ionization chamber (TN 30013, PTW, Freiburg, Germany) placed at the center of the water-equivalent phantom. The first beam was configured using 50 kVp and 14.4 mA and the second beam was set to 25 kVp with 34.5 mA. Irradiations were carried out with a 30×30 mm^2 field size, a source-to-phantom distance of ₁₂₅ 930 mm and a collimator to sample distance of 135 mm. Secondly, to study the fluorescence detection in Fricke gel dosimeters, the Ag NPs products were placed inside polymethylmethacrylate (PMMA) cuvettes within a poly(ethylene terephthalate) (PET) phantom. These samples were irradiated configuring the setup as described elsewhere [16] delivering the same total dose (12 Gy). The

7

130 scattered spectrum was detected by an AMPTEK XR-100T Cd-Te γ/X-ray detector. The distance from the phantom's surface to the surface of the volume doped with Ag was 1 mm and the silver concentration was varied from 0.005 to 0.05 M.

3. Results and discussion

3.1. Reaction product and purification process

In order to study the reaction product, a DLS analysis was carried out and obtained results are depicted in Figure 2. Size distribution of gelatin-silver complex structures in a typical reaction product (sample G5) can be observed in this figure, presenting a monomodal distribution with a polydispersity index of

140 0.22, mean size of 120.4 nm, standard deviation of 57.8 nm and maximum size of 317.8 nm. To prove weather an interaction between the gelatin and silver nitrate salt or Ag NPs exists, a reaction mixture was processed under equivalent conditions but with no silver nitrate. The DLS of this reaction product presents a multimodal distribution with a polydispersity index of 0.31, a domi-

145 nant mean size distribution centered on 311.8 nm, standard deviation of 155.2 nm and a maximum size of 843.5 nm. It is worthwhile mentioning, that multimodal distributions are not accurately measured by DLS, but they can provide information on the stabilization and complex macromolecular structure formed in the presence of silver nitrate.
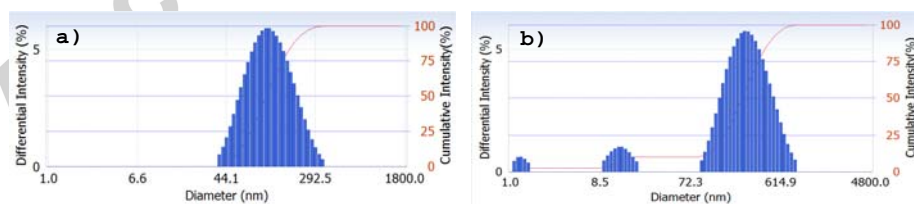

Figure 2: DLS results for G5 **(a)** and equivalent sample (48 mM gelatin concentration and 15 h reaction time) but without silver nitrate **(b)**.

150 As previously described, a purification process was required to eliminate the remaining inorganic salt and to obtain a suitable product for gel dosimetry
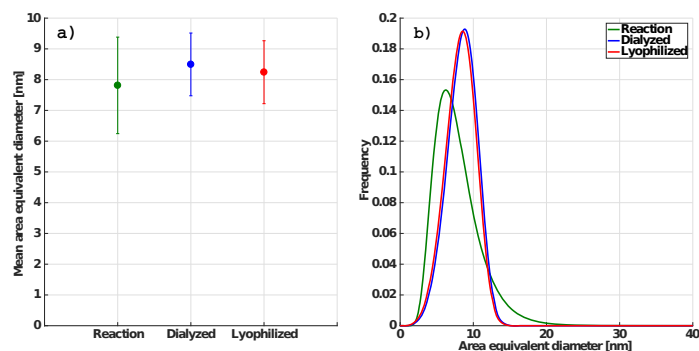
8

Figure 3: TEM results for the reaction product (G5) and during its two-steps purification process.

applications. Therefore, dialysis and freeze drying process of the synthesis product were carried out. In order to check if size distribution was not modified by these purification processes, mean particle sizes of the reaction product before ₁₅₅ and after each process were measured by TEM. The results are presented in Figure 3 confirming that no significant changes in the mean particle size were observed in the dialysis process detecting only a loss of the smaller particles, thus resulting in a narrower size distribution changing their mean particle size from 7.81 to 8.50 nm. The lyophilization process didn't have any influence over ₁₆₀ the mean particle size distribution. With these results it is demonstrated that the purification process has no significant effect on the homogeneity of the Ag NPs suspension.

3.2. Particle size distribution from TEM images

In order to analyze the effect of synthesis variables in the use of Ag NPs in ₁₆₅ theranostics, it is necessary to have a properly description of the particle's size distribution. Particle size histograms were obtained from TEM images for each synthesis product by means of the previously described method. This method relays on contrast differences in TEM images, in which a minimum area needs to be specified to avoid including image noise as particles. The minimum particle ₁₇₀ area was set to 9 nm^2, the sensitivity analysis of this parameter is included as

9

supplementary information in Appendix B.

According to Rice *et al* [20] the most common models for nanoparticle size distributions are Normal, Lognormal and Weibull. These distribution models have two parameters, related to the size and the shape of the distribution. With the aim of describing accurately the distributions of the particles obtained in this study, these models were tested on different samples. The fitting was assessed by the Kolmogorov-Smirnov test [22]. Figure 4 shows the results for the different models on sample G2, where a three-parameter distribution (Burr Type XII) was also included for comparison purposes. A probability plot, a plot that includes a reference line useful for judging whether the data follows the distribution, was made for graphic visualization of each distribution fit. The general equations of the used fitting distribution are Equation 1 for Lognormal, Equation 2 for Weibull and Equation 3 for Burr Type XII:

$$f\left(x|\mu,\sigma\right) = \frac{1}{x\sigma\sqrt{2\pi}}\exp\left[\frac{-\left(\ln(x)-\mu\right)^2}{2\sigma^2}\right] \qquad x > 0 \tag{1}$$

$$f\left(x|a,b\right) = \frac{a}{b}\left(\frac{x}{a}\right)^{b-1}\exp\left[-\left(\frac{x}{a}\right)^b\right] \tag{2}$$

$$f\left(x|\alpha,c,k\right) = \frac{ck}{\alpha}\left(\frac{x}{\alpha}\right)^{c-1}\left(1+\left(\frac{x}{\alpha}\right)^c\right)^{-(k+1)} \qquad x,\alpha,c,k > 0 \tag{3}$$

As suggested by other authors [25, 20], the best fit to represent the area equivalent diameter of most of the obtained particles is the Lognormal distribution, which has the best p-value (0.4759) among the four fitted functions. Therefore, a Lognormal distribution was used to fit the particle size distribution of all samples, except for those whose p-values were lower than 0.05. Obtained results for all samples analyzed in this study are detailed in Table 2.
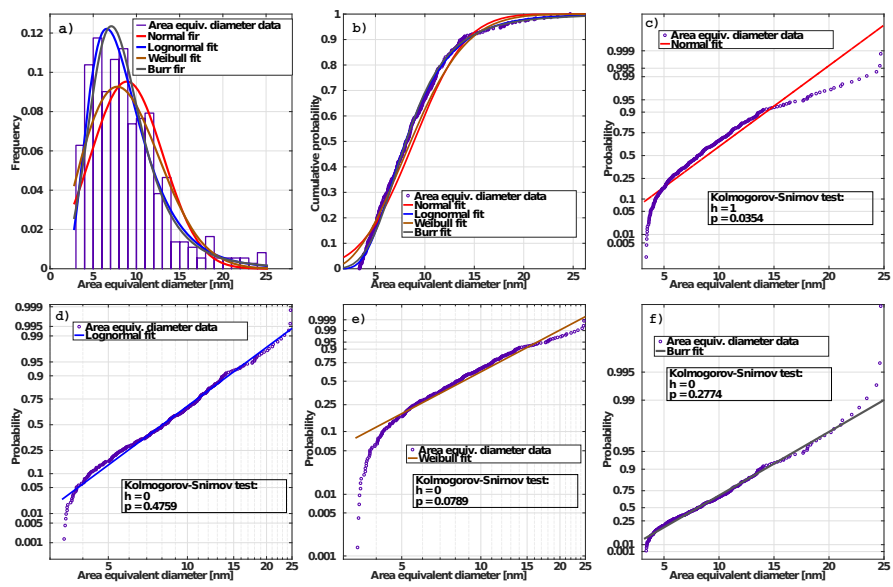
10

Figure 4: Fitted particle size distribution of sample G2. **a)** Area equivalent diameter histogram and the studied fits. **b)** Cumulative distribution plots. Also, each probability plot is shown together with the Kolmogorov-test results. **c)** Normal fit. **d)** Lognormal fit. **e)** Weibull fit. **f)** Burr fit.

11

Table 2: Results obtained by TEM images analysis. Each fit parameter is shown. All distribution accepted the null hypothesis in the Kolmogorov-Smirnov test ($h = 0$). "Par." stands for parameter, "Size" stands for mean area equivalent diameter and "St. dev." stands for standard deviation.

Studied variable	Synthesis ID	Particle number	Fitted distribution	Par. A (*)	Par. B (**)	p-value	Size [nm]	St. dev. [nm]
Purification	G5	275	Lognormal	1.981	0.3968	0.3800	7.809	3.137
process	G5 - dialyzed	720	Wiebull	9.280	4.7500	0.0806	8.496	2.039
	G5 - lyophilized	824	Wiebull	9.023	4.5770	0.0672	8.242	2.046
Reaction	G1 - T1	375	Lognormal	2.284	0.4792	0.4593	11.014	5.596
time	G1 - T2	255	Lognormal	1.941	0.3898	0.5759	7.519	3.046
variation	G1 - T3	682	Lognormal	2.069	0.4525	0.1254	8.773	4.182
	G2 - T1	302	Lognormal	2.081	0.3955	0.5514	8.662	3.564
	G2 - T2	305	Lognormal	2.184	0.4219	0.6059	9.704	4.283
	G2 - T3	563	Burr (***)	11.31	5.317	0.3325	11.043	3.532
AgNO₃	A1	157	Lognormal	2.544	0.5855	0.0504	15.100	9.658
variation	A2	302	Lognormal	2.081	0.3955	0.5514	8.662	3.564
	A3	457	Lognormal	2.041	0.4019	0.7218	8.307	3.354
Gelatin	G1	375	Lognormal	2.284	0.4792	0.4593	11.014	5.596
concentration	G2	302	Lognormal	2.081	0.3955	0.5514	8.662	3.564
variation	G3	704	Lognormal	1.872	0.3618	0.0948	6.938	2.594
	G4	180	Lognormal	2.036	0.4009	0.7106	8.297	3.465
	G5	275	Lognormal	1.981	0.3868	0.3800	7.809	3.137
	G6	272	Lognormal	2.210	0.3587	0.8012	9.721	3.602

(*) Parameter A respectively represents μ, a and α for Lognormal, Weibull and Burr fits.

(**) Parameter B respectively represents σ, b and c for Lognormal, Weibull and Burr fits.

(***) Parameter k = 1.281 for Burr fit.

190   For theranostic applications it is desirable to have uniformly distributed NPs in the whole target volume. Hence, smaller particles size and narrower distributions are preferred and synthesis conditions that lead to such characteristics should be used.

3.3. UV-Vis spectroscopy

195   Typical spectral UV-Vis curves of Ag NPs colloidal suspensions are shown in Figure 5. Their characteristic band of surface plasmon resonance appears centered near 420 nm, which supports the formation of Ag NPs. Also, the extinction maximum value and shape of the spectrum can be associated with the total surface area of nanoparticles [26]. Nevertheless, a quantitative anal-
200   ysis of the particles size distribution can not be made directly from this type of results and only some qualitative information can be obtained from them. For example, the average mean size of the nanoparticles has a direct relationship with the wavelength where the maximum in the extinction peak is located, obtaining larger wavelengths for larger particles. Moreover, the height of the
205   extinction peak is intimately related to the total surface of nanoparticles, thus a higher nanoparticles content or a smaller size leads to a higher total surface and consequently to a higher extinction peak. Figure 5 a) shows that the surface plasmon resonance band linearly increases together with the reaction time, which is associated to the fact that a higher number of Ag NPs leads to a greater
210   specific surface area. In addition, Figure 5 b) exhibits that the extinction value increases while the maximum wavelength decreases when a longer reaction time is used. Therefore, a higher Ag NPs amount with a lower size was obtained. This behavior could be related to the fact that nucleation kinetics are higher than that of particle growth processes under these conditions. Before thermal
215   process the amino group of gelatin gets complexes with the silver ions, placing the latter into reaction center. These complexes of silver ion/gelatin avoid the ions diffusion during Ag NPs formation, which favors the nucleation process.
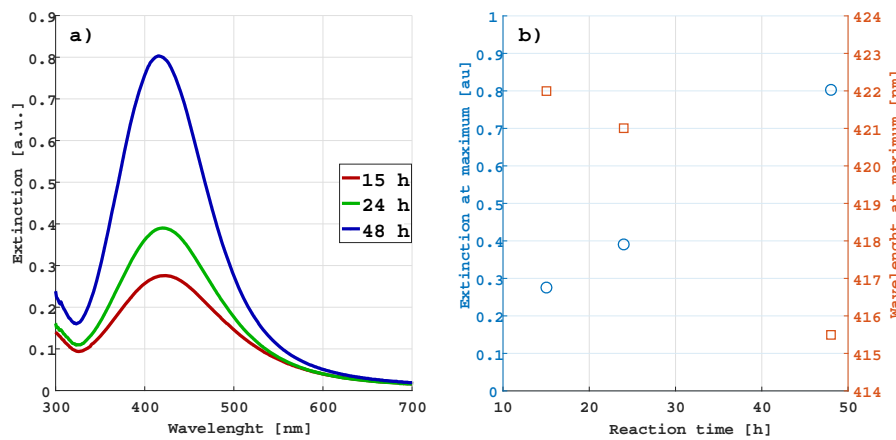
13

Figure 5: Spectral UV-Vis curves for Ag NPs colloidal suspension synthesized from a 50 mM of silver nitrate and a 8 mM of gelatin aqueous solution for different reaction times. **a)** Extinction spectra. **b)** Extinction value at maximum and its corresponding wavelength.

3.4. Assessment of synthesis variables

In the following subsections, extinction peak height and its corresponding ₂₂₀ wavelength are analyzed together with TEM results and synthesis yield to study the effect of the synthesis variables on the final reaction product morphological characteristics.

It is worth pointing out that in TEM analysis samples were dried over TEM grids, hence gelatin particles loose their water content shrinking their volume. ₂₂₅ the final particles measured by TEM represents the size of dry gelatin particle containing Ag NPs. Therefore, size distributions determined by TEM images suggest larger dimensions than the actual size of Ag NPs.

3.4.1. Effect of reaction time on the synthesis performance

In order to study the influence of the reaction time in the NPs synthesis ₂₃₀ process, initial silver nitrate concentration was kept constant at 50 mM (experiments G1-T1 to G2-T3 in Table 1). When the reaction time was varied, two different behaviors were observed depending on the gelatin concentration. The resulting trends and behaviors can be observed in Figure 6 as black trian-

14

gles (8 mM of gelatin) and green circles (16 mM of gelatin), respectively. For
235   the lowest gelatin concentration and shortest reaction time a less homogeneous
product with a poor stability was obtained, the overall reaction yield was 12.87
mol-%, indicating that very few Ag NPs were formed. As a consequence, less
gelatin complexation with Ag NPs was present leading to less reproducibility
and larger deviations in the particle size of the final product, as it can be seen
240   in the TEM analysis in Figure 6. On the other hand, reaction times larger than
24 h provided quite similar product stabilities. In both gelatin concentrations
reaction products presented similar trends, but a minimum yield was required
to assure product stability in all cases. Longer reaction times lead to larger
complex products as it can be observed from the TEM results, but with smaller
245   Ag NPs indicated by changes in the wavelength of the plasmonic signal from
the UV-Vis analysis and higher reaction yields. For illustrative purpose, TEM
images of samples G1-T1 to G1-T3 are shown in Figure 7.

3.4.2. Synthesis yield as a function of silver nitrate concentration

In these series, gelatin concentration was kept constant at 16 mM (experi-
250   ments A1 to A3 in Table 1). Obtained results are depicted in Figure 8. Once
again, conditions that led to very low reaction yields (34.29 mol-%) produced
unstable particles with large deviations and poor reproducibility. In this case
the lowest silver nitrate concentration presented this behavior, while the other
two concentrations resulted in stable products with reliable properties. In these
255   experiments, no significant variations were observed on the compound particle
average size obtained in the TEM analysis. Nevertheless, in the UV-Vis results
non-negligible changes were observed between the unstable and stable products,
where the average size of Ag NPs increased as reflected in the wavelength shift
of the extinction maximum from 423 nm to 427 nm. Once the product is stable,
260   the silver nitrate concentration had no significant effect on the compound parti-
cle size or Ag NPs size. The reaction efficiency always increased for higher silver
nitrate concentrations, as observed from the extinction peak changes through
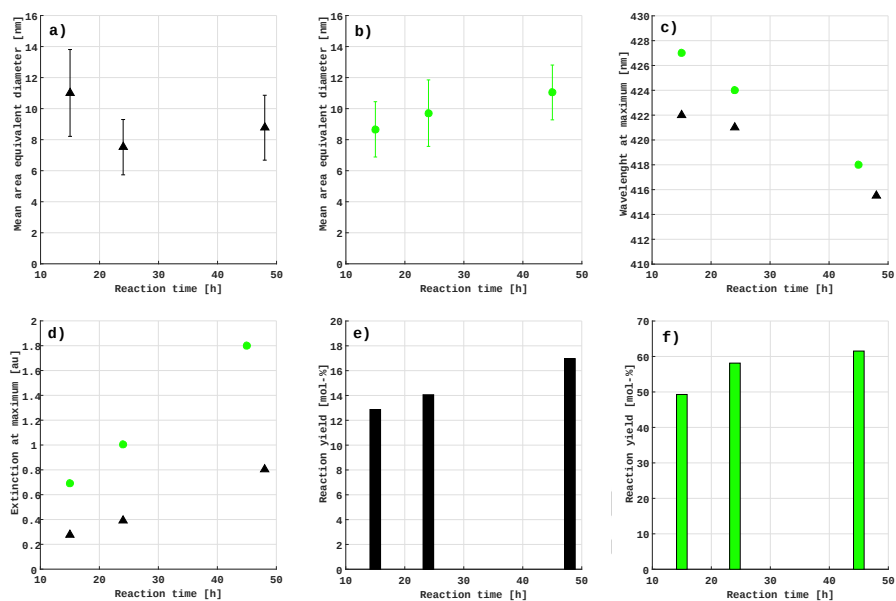the series. In summary, a minimum silver nitrate concentration was necessary

15

Figure 6: Synthesis reaction time study. Silver nitrate concentration was set to 50 mM for all the experiments. Two gelatin concentrations were used: 8 mM (black) and 16 mM (green). **a)** and **b)** Mean area equivalent diameter obtained by TEM analysis. UV-Vis results: **c)** wavelength location of extinction maximums and **d)** maximum extinction values. **e)** and **f)** Yields of Ag NPs synthesis.
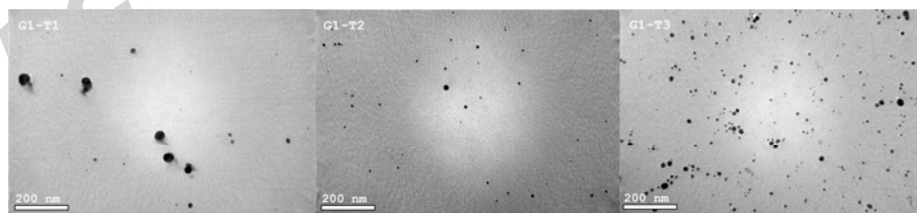

Figure 7: TEM images for synthesis reaction time study with 8 mM of gelatin and 50 mM of AgNO$_3$.

16
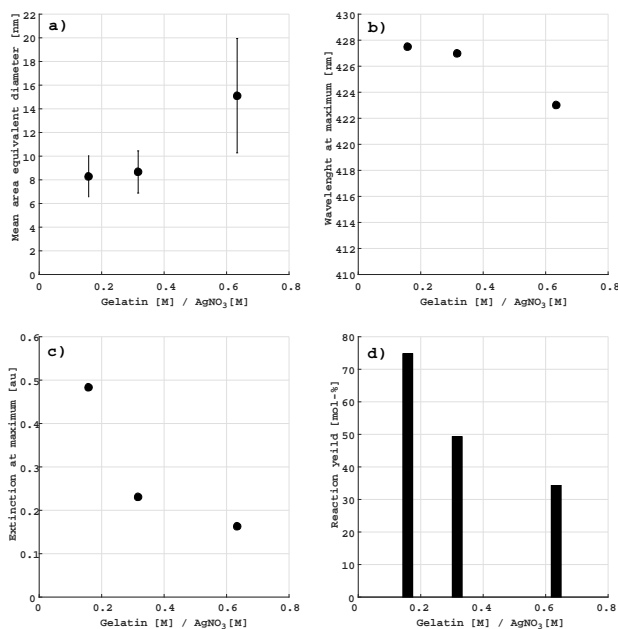
Figure 8: Silver nitrate concentration study for different gelatin/AgNO$_3$ molar ratios. Gelatin concentration was set to 16 mM for all experiments. **a)** Mean area equivalent diameter obtained by TEM analysis. **b)** Wavelength location of the plasmonic extinction peak in UV-Vis results. **c)** Maximum extinction value in UV-Vis results. **d)** Reaction yield of Ag NPs synthesis.

to obtain a stable product, while values higher than 50 mM of AgNO$_3$ (a 0.3
265 molar ratio of gelatin/AgNO$_3$) had no significant effect on the particle size but led to higher reaction yields. For illustrative purposes, TEM images of samples A1 to A3 are shown in Figure 9.

3.4.3. Gelatin concentration influence in the performance of Ag NPs formation

Two different series were studied for two different silver nitrate concentra-
270 tions (experiments G1 to G6 in Table 1), a value of 50 mM of AgNO$_3$ was used as the "low concentration value" and of 150 mM as the "high concentration value". In both series, different gelatin concentrations were used while keeping the same molar ratio and reaction times of 15 h. The results are presented in Figure 10, the synthesis with the lowest concentration led to unstable products
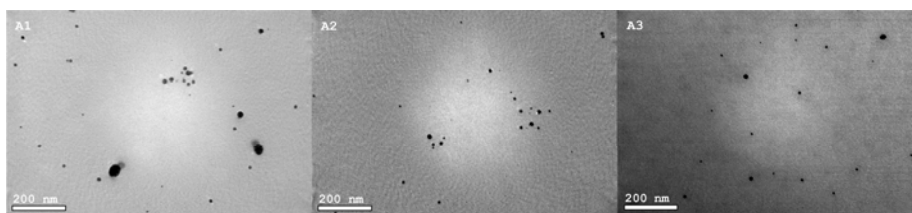
17

Figure 9: TEM images for the silver nitrate concentration study.

275 with a reaction yield lower than 12.87 mol-%. In this study, two opposite behaviors were observed depending on the silver nitrate concentration. When the lowest silver nitrate concentration was used, the average size of the compound product decreased as gelatin concentration increased also showing a narrower size distribution. However, for the highest silver nitrate concentration the mean 280 area equivalent diameter slightly increased when increasing the gelatin concentration with no other significant effect on the Ag NPs average size. The reaction yield increased in both series when the gelatin concentration was increased. For illustrative purposes, TEM images of samples G4 to G6 are shown in Figure 11.

All the presented results were used to define the synthesis conditions for 285 the production of the Ag NPs used in the Fricke gel dosimeters, namely silver nitrate concentration of 150 mM, gelatin concentration of 48 mM and a reaction time of 15 hours.

3.5. X-ray applications

In terms of the proposed goals in the present study, the feasibility of using 290 the synthesized Ag NPs in theranostic applications with X-rays was studied and analyzed by two different set of experiments. First, fluorescence detection of soft tissue equivalent phantoms doped with the synthesis products was assayed and the results are presented in Figure 12 a). As expected, emergent radiation from the irradiated volume revealed the characteristic fluorescent emissions, namely 295 photons due to K_α and K_β transitions, thus evidencing the presence of Ag within the irradiated volume. Moreover, an unambiguous linear relationship (r^2=0.9991) between silver concentration and relative intensity K_α lines was
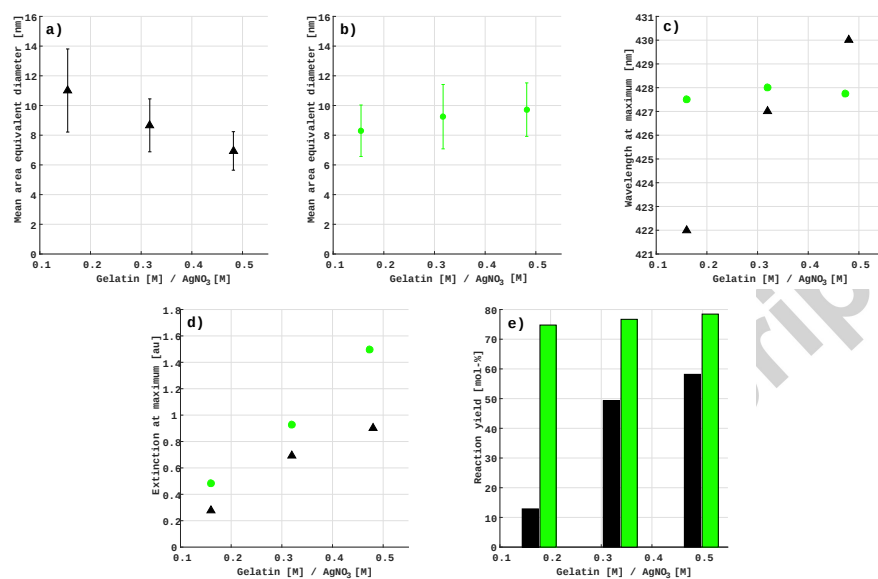
18

Figure 10: Gelatin concentration study for different gelatin/AgNO$_3$ molar ratios. Silver nitrate concentration of 50 mM was set in the first series represented in black and 150 mM in the second series represented in green. **a)** and **b)** Mean area equivalent diameter obtained by TEM analysis. **c)** Wavelength location of the plasmonic extinction peak in UV-Vis results of both series. **d)** Maximum extinction value in the UV-Vis results. **e)** Yields of Ag NPs synthesis.
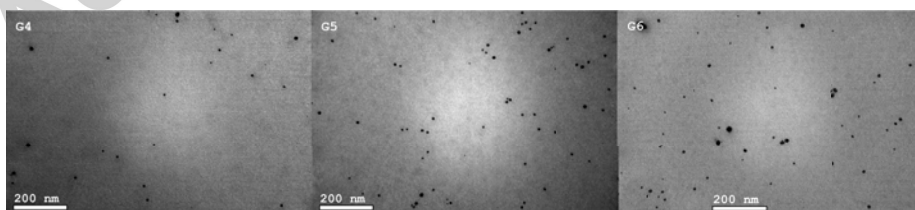

Figure 11: TEM images for synthesis gelatin concentration study with 150 mM of AgNO$_3$.
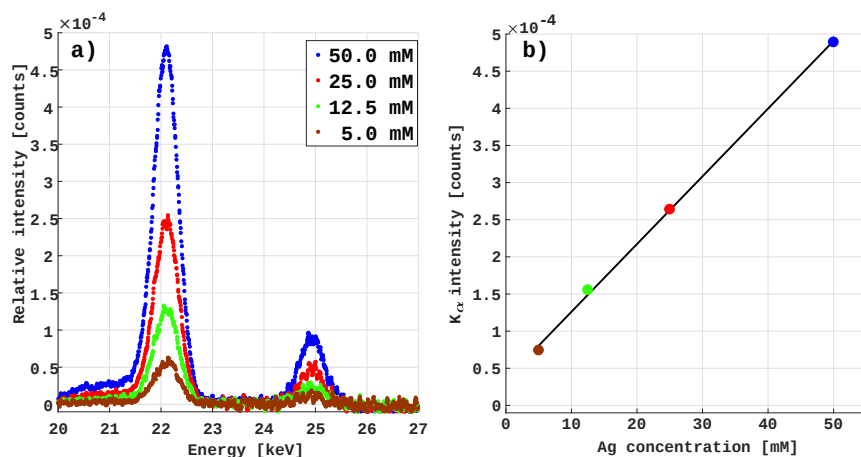
19

Figure 12: Synthesized Ag NPs in theranostics X-ray applications. **a)** Fluorescence detection for different silver concentrations (weighted over three samples, statistical uncertainties are less than 3%). **b)** K_α maximum intensity versus silver concentration (circles) and linear fit (solid line).

obtained, as reported in Figure 12 b). According to these results, it may be possible to use emergent radiation to assess practical correlations for the estimation of the concentration and location of Ag NPs aimed at diagnosis purposes.

300

Secondly, the difference in the absorbance of Fricke gel dosimeters irradiated below and above silver K-edge was studied. As known, dose enhancement due to secondary electrons is a consequence of excitations of the internal bound of Ag electrons. Therefore, incident X-ray beams with energies capable of exciting Ag

Table 3: Dose-response (absorbance change) for silver nanoparticle-infused Fricke gel dosimeters irradiated above and below silver K-edge.

NPs	X-ray beam	Absorbance change [au]		
[mM]	[kVp]	$\lambda = 585$ nm	$\lambda = 595$ nm	$\lambda = 605$ nm
0	25	0.022 ± 0.003	0.017 ± 0.005	0.011 ± 0.006
0	50	0.025 ± 0.003	0.019 ± 0.004	0.013 ± 0.006
10	25	0.113 ± 0.002	0.115 ± 0.002	0.116 ± 0.003
10	50	0.164 ± 0.002	0.166 ± 0.003	0.168 ± 0.003

20

305 K-edge (25.5 keV) shall be able to produce the extra contribution to total dose called "dose enhancement". The local dose enhancement due to the presence of Ag NPs was evidenced by comparisons of standard and nanoparticles-infused Fricke gel dosimeters being irradiated with incident spectra capable or not of exciting the silver K-edge, as summarized in Table 3. This table reports ab-

310 sorbance changes averaged over three samples at different wavelengths. As expected, for silver nanoparticle-infused Fricke gel dosimeters absorbance changes increase when dosimeters are irradiated above K-edge, which may be attributed to the secondary de-excitation electrons emitted by Ag atoms. Therefore, this extra absorbance change may correspond to the initially predicted "dose en-

315 hancement" effect.

4. Conclusions

A green nanoparticles synthesis process was proposed and developed to obtain Ag NPs stable and compatible with Fricke gel dosimetry for further applications in theranostics. With this synthesis method, it was possible to control

320 the particle size by changing the reaction variables. Minimum necessary concentrations and reaction times to obtain stable silver nanoparticle-gelatin complex structures have been defined based on the obtained results. For typical synthesis conditions, particles with a mean size of 120 nm containing Ag NPs of less than 10 nm can be obtained with a reaction yield of at least 76.70 mol-%.

325 Finally, the obtained synthesis products were successfully used for preliminary theranostics applications, acting as fluorescent agent in X-ray beam irradiations. Emerging radiation was successfully detected evidencing the presence of Ag NPs by means of the characteristic silver K-lines and the good correlation between K_α peaks and Ag NPs concentrations. Besides, the proof of concept

330 of using these nanoparticles as dose enhancer in Fricke gel dosimetry has been stated by detecting a difference in the registered signal of Fricke gel dosimeters doped with Ag NPs when they were irradiated above and below the silver K-edge.

21

To the authors' knowledge, the obtained results represent the first conclusive
335 experimental confirmation of the use of green synthesized Ag NPs in theranostics. Furthermore, these NPs have been proved useful as dose enhancers in a Fricke gel dosimeter, as well as on-line monitoring devices by detecting emerging radiation due to the presence of nanoparticles.

Acknowledgements

Appendix A. Reaction yield estimation method

In order to estimate the yield of nanoparticles synthesis and their concentration in the dialyzed product, a quantification method using ascorbic acid (p.a. from Anedra, Argentina) was proposed. The method consisted on obtaining 350 the concentration of the unreacted silver ions in, either the final product or the dialysis water, performing the following steps:

   a. A solution of ascorbic acid in a acetic acid buffer solution with a pH of 4 was prepared 2 hours previous to the analytical assay.

   b. The sample of interest and the ascorbic acid solution were mixed in a 1:2.7 volumetric ratio and kept at 25 ℃ in a dark room for 60 minutes. Within this time, the reduction of the silver ions with ascorbic acid took place. Due to the relative expected concentration, all the silver ions were consumed and turned into metallic silver according to the following stoichiometry:

$$2Ag^+ + C_6H_8O_6 \rightarrow 2Ag + C_6H_6O_6 + 2H^+$$

22

<p style="text-align:right;">355</p>
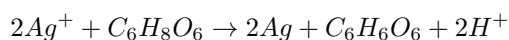
c. The obtained Ag NPs suspension was then centrifuged for 10 minutes at 8000 rpm in a Rolco CM-2050 (Argetnina) centrifuge to separate the metallic silver from the ascorbic acid solution.

d. The supernatant was then diluted in a acetic acid buffer (7.5e-4 M, pH: 4) in a 1:50 ratio and the ascorbic acid concentration was then measured by UV-Vis spectroscopy in a Shimadzu UV-1800 spectrophotometer (Japan) and a quantitative analysis can be made with the appropriate calibration curve.

When the the reaction product was analyzed, in order to separate the Ag NPs from silver ion solution, the sample was previously centrifuged for 30 minutes at 8000 rpm.

Appendix B. Sensitivity analysis of the minimum particle size

The method used to obtain the particle size distribution from TEM images relays on image contrast differences for particle identification. Since NPs obtained in this study are contained in a gelatin matrix, in some cases particles were identified in regions where only gelatin was present. This limitation was noticeable for particles with a diameter lower than 5 nm. Therefore, the effect of omitting particles below a certain size in the analysis was evaluated by varying the minimum considered particle size from 1 to 11 nm^2 (equivalent diameter from 1.28 to 3.74 nm). The results are depicted in Figure B.13, Figure B.14, Figure B.15 and Figure B.16.

If the minimum particle area selection is too small, the noise in TEM images are considered as particles. Thus, the histogram becomes positively skewed and not representative of the distribution in the sample. On the other hand, if the minimum particle is too large many particles form the distribution becomes omitted and the distribution shape also becomes not representative of the whole sample. A compromise situation exists, in this study a minimum size of 9 nm^2 was selected, because of the high obtained p-value and also due to the
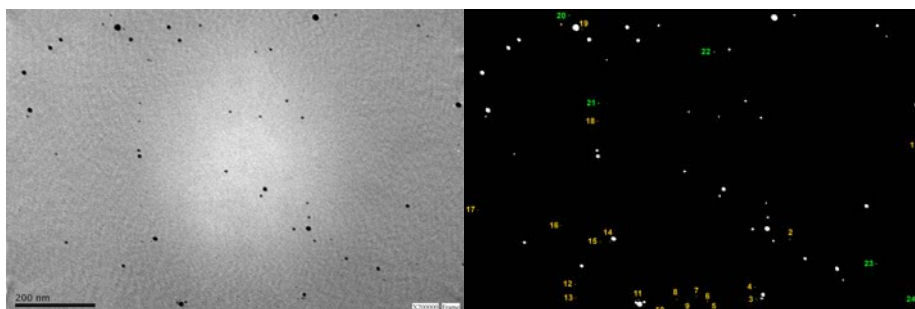
23

Figure B.13: Minimum particle size analysis. TEM image of sample G2 is shown on the left and on the right the result of ImageJ particle analysis with different minimum particle areas: for 3 nm^2 all particles (whites, greens and yellows) were detected, for 7 nm^2 particles number from 1 to 19 were omitted (in yellow) and for 11 nm^2 also particles from 20 to 24 were omitted (in green).
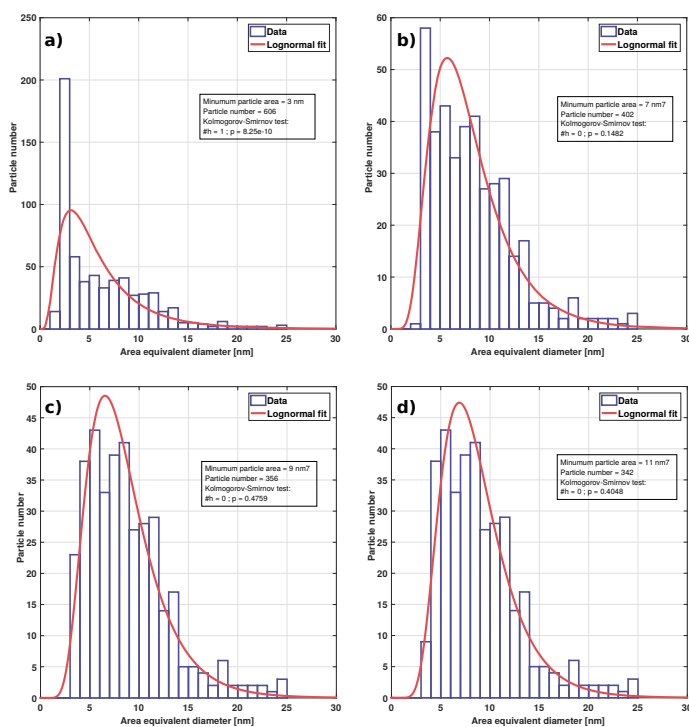

Figure B.14: Histograms and Lognormal fits for sample G2 with minimum particle area 3 nm^2 (a), 7 nm^2 (b), 9 nm^2 (c) and 11 nm^2 (d).
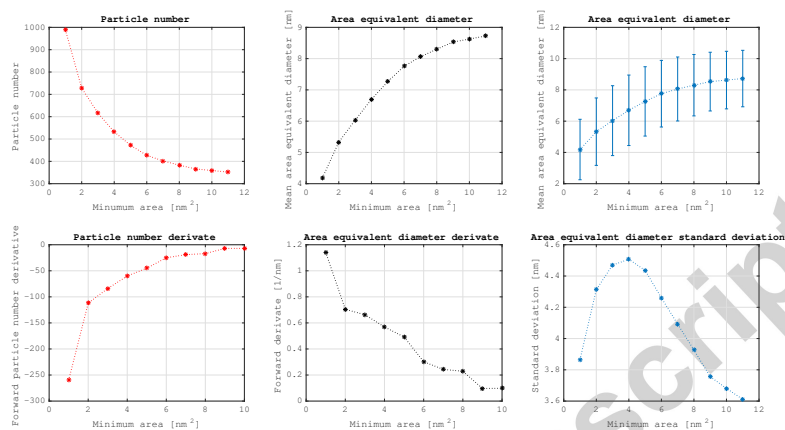
24

Figure B.15: Complete analysis of minimum particle area selection from 1 to 11 nm^2. Reported results correspond to TEM images analysis of G2 sample.
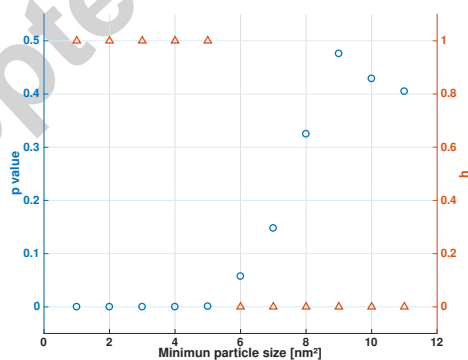

Figure B.16: Kolmogorov-Smirnov test results for the different minimum particle area selection and p-value of the Lognormal fits. Reported results correspond to TEM images analysis of sample G2.

25

stabilization on the trend of particle number and area equivalent average mean diameter with the variation on the minimum particle area observed for that value.

385 **References**

[1] M. Kulkarni, A. Mazare, E. Gongadze, Š. Perutkova, V. Kralj-Iglič, I. Milošev, P. Schmuki, A. Iglič, M. Mozetič, Titanium nanostructures for biomedical applications, Nanotechnology 26 (6) (2015) 062002. `doi: 10.1088/0957-4484/26/6/062002`.

390 [2] S. Goswami, H. Pant, J. Biswal, J. Samantray, V. Sharma, A. Dash, Synthesis, characterization and application of Au-198 nanoparticles as radiotracer for industrial applications, Appl. Radiat. Isotopes 111 (2016) 18–25. `doi:10.1016/j.apradiso.2016.01.028`.

[3] M. Cushen, J. Kerry, M. Morris, M. Cruz-Romero, E. Cummins, Nanotech-
395 nologies in the food industry–Recent developments, risks and regulation, Trends Food Sci. Tech. 24 (1) (2012) 30–46. `doi:10.1016/j.tifs.2011. 10.006`.

[4] S. Küünal, S. Kutti, P. Rauwel, M. Guha, D. Wragg, E. Rauwel, Biocidal properties study of silver nanoparticles used for application in
400 green housing, Int. Nano. Lett. 6 (3) (2016) 191–197. `doi:10.1007/ s40089-016-0186-7`.

[5] M. L. Etheridge, S. A. Campbell, A. G. Erdman, C. L. Haynes, S. M. Wolf, J. McCullough, The big picture on nanomedicine: the state of investigational and approved nanomedicine products, Nanomedicine: nanotechnol-
405 ogy, biology and medicine 9 (1) (2013) 1–14. `doi:10.1016/j.nano.2012. 05.013`.

[6] M. Hassoun, I. W. Schie, T. Tolstik, S. E. Stanca, C. Krafft, J. Popp, Surface-enhanced Raman spectroscopy of cell lysates mixed with silver

26

nanoparticles for tumor classification, Beilstein J. Nanotechnol. 8 (1) (2017) 1183–1190. doi:10.3762/bjnano.8.120.

[7] M. Krukemeyer, V. Krenn, F. Huebner, W. Wagner, R. Resch, History and possible uses of nanomedicine based on nanoparticles and nanotechnological progress, J. Nanomed. Nanotechnol. 6 (6) (2015) 1. doi: 10.4172/2157-7439.1000336.

[8] N. Supraja, T. Prasad, T. G. Krishna, E. David, Synthesis, characterization, and evaluation of the antimicrobial efficacy of Boswellia ovalifoliolata stem bark-extract-mediated zinc oxide nanoparticles, Appl. Nanosci. 6 (4) (2016) 581–590. doi:10.1007/s13204-015-0472-0.

[9] J. Lin, M. Wang, H. Hu, X. Yang, B. Wen, Z. Wang, O. Jacobson, J. Song, G. Zhang, G. Niu, P. Huang, Multimodal-Imaging-Guided Cancer Phototherapy by Versatile Biomimetic Theranostics with UV and γ-Irradiation Protection, Adv. Mater. 28 (17) (2016) 3273–3279. doi: 10.1002/adma.201505700.

[10] P. Huang, L. Bao, C. Zhang, J. Lin, T. Luo, D. Yang, M. He, Z. Li, G. Gao, B. Gao, S. Fu, D. Cui, Folic acid-conjugated silica-modified gold nanorods for X-ray/CT imaging-guided dual-mode radiation and photothermal therapy, Biomaterials 32 (36) (2011) 9796–9809. doi:10.1016/j. biomaterials.2011.08.086.

[11] K. Ricketts, C. Guazzoni, A. Castoldi, A. Gibson, G. Royle, An x-ray fluorescence imaging system for gold nanoparticle detection, Phys. Med. Biol. 58 (21) (2013) 7841. doi:10.1088/0031-9155/58/21/7841.

[12] N. Manohar, F. J. Reynoso, P. Diagaradjane, S. Krishnan, S. H. Cho, Quantitative imaging of gold nanoparticle distribution in a tumor-bearing mouse using benchtop x-ray fluorescence computed tomography, Scientific reports 6 (2016) 22079. doi:10.1038/srep22079.

27

[13] B. L. Jones, S. Krishnan, S. H. Cho, Estimation of microscopic dose enhancement factor around gold nanoparticles by Monte Carlo calculations, Med. Phys. 37 (7) (2010) 3809–3816. doi:10.1118/1.3455703.

[14] E. Porcel, S. Liehn, H. Remita, N. Usami, K. Kobayashi, Y. Furusawa, C. Le Sech, S. Lacombe, Platinum nanoparticles: a promising material for future cancer therapy?, Nanotechnology 21 (8) (2010) 085103. doi: 10.1088/0957-4484/21/8/085103.

[15] C. Baldock, Review of gel dosimetry: a personal reflection, in: J. Phys. Conf. Ser., Vol. 777, IOP Publishing, 2017, p. 012029. doi:10.1088/1742-6596/777/1/012029.

[16] F. Mattea, J. Vedelago, F. Malano, C. Gomez, M. C. Strumia, M. Valente, Silver nanoparticles in x-ray biomedical applications, Radiat. Phys. Chem. 130 (2017) 442–450. doi:10.1016/j.radphyschem.2016.10.008.

[17] M. Naghdi, M. Taheran, S. K. Brar, M. Verma, R. Surampalli, J. Valero, Green and energy-efficient methods for the production of metallic nanoparticles, Beilstein J. Nanotechnol. 6 (2015) 2354. doi:10.3762/bjnano.6.243.

[18] J. Krstić, J. Spasojević, A. Radosavljević, M. Šiljegović, Z. Kačarević-Popović, Optical and structural properties of radiolytically in situ synthesized silver nanoparticles stabilized by chitosan/poly (vinyl alcohol) blends, Radiat. Phys. Chem. 96 (2014) 158–166. doi:10.1016/j.radphyschem.2013.09.013.

[19] M. Bin Ahmad, J. J. Lim, K. Shameli, N. A. Ibrahim, M. Y. Tay, Synthesis of silver nanoparticles in chitosan, gelatin and chitosan/gelatin bio-nanocomposites by a chemical reducing agent and their characterization, Molecules 16 (9) (2011) 7237–7248. doi:10.3390/molecules16097237.

[20] S. B. Rice, C. Chan, S. C. Brown, P. Eschbach, L. Han, D. S. Ensor, A. B. Stefaniak, J. Bonevich, A. E. Vladár, A. R. H. Walker, Par-

28

ticle size distributions by transmission electron microscopy: an inter-
₄₆₅ laboratory comparison case study, Metrologia 50 (6) (2013) 663. `doi:
10.1088/0026-1394/50/6/663`.

[21] C. A. Schneider, W. S. Rasband, K. W. Eliceiri, NIH Image to ImageJ: 25
years of image analysis, Nat. Methods 9 (7) (2012) 671–675. `doi:10.1038/
nmeth.2089`.

₄₇₀ [22] F. J. Massey Jr, The Kolmogorov-Smirnov test for goodness of fit, J.
Am. Stat. Assoc. 46 (253) (1951) 68–78. `doi:10.1080/01621459.1951.
10500769`.

[23] J. Vedelago, D. Chacón Obando, F. Malano, R. Conejeros, R. Figueroa,
D. Garcia, G. González, M. Romero, M. Santibañez, M. Strumia,
₄₇₅ J. Velásquez, F. Mattea, M. Valente, Fricke and polymer gel 2D dosimetry
validation using Monte Carlo simulation, Radiat. Meas. 91 (2016) 54–64.
`doi:10.1016/j.radmeas.2016.05.003`.

[24] S. Triviño, J. Vedelago, F. Cantargi, W. Keil, R. Figueroa, F. Mattea,
A. Chautemps, M. Santibañez, M. Valente, Neutron dose estimation in a
₄₈₀ zero power nuclear reactor, Radiat. Phys. Chem. 127 (2016) 62–67. `doi:
10.1016/j.radphyschem.2016.06.011`.

[25] F. L. Deepak, A. Mayoral, R. Arenal, Advanced Transmission Electron
Microscopy: Applications to Nanomaterials, Springer, 2015. `doi:10.1007/
978-3-319-15177-9`.

₄₈₅ [26] K. L. Kelly, E. Coronado, L. L. Zhao, G. C. Schatz, The optical properties
of metal nanoparticles: the influence of size, shape, and dielectric environ-
ment, J. Phys. Chem. B 107 (3) (2003) 668–667. `doi:10.1021/jp026731y`.